Reducing Motion Artifacts in 3-D Breast Ultrasound Using Non-linear Registration

Tobias Boehler and Heinz-Otto Peitgen

MeVis Research, Bremen, Germany
tobias.boehler@mevis.de

Abstract. Automated full-field 3-D breast ultrasound (3DBUS) has a high potential as a reproducible method for screening and intervention. Consecutive linear transducer scans yield a consistent breast ultrasound volume, yet individual slices are prone to tissue deformation and motion. To compensate resulting image distortions, we propose an efficient non-rigid registration method applied sequentially to pairs of 3DBUS volume slices, optionally either on-line or in post-processing. A quantitative evaluation of the method on synthetic deformations shows subvoxel registration accuracy. First application to clinical breast US images and preliminary results confirmed effectiveness and accuracy of the method.

1 Introduction

Diagnostics of breast cancer in routine clinical screening relies primarily on conventional X-ray mammography (MG), due to its high sensitivity, distinct spatial resolution and common availability. Standard MG diagnostics allow the detection of large lesion masses as well as of diminutive microcalcifications. However, increased breast density impedes lesion diagnostics. Thus, individual interpretation of mammograms is often supplemented by further ultrasound (US) examinations employing 2-D ultrasound systems and hand-held transducer units. This established combination has proven to gain valueable insight into lesion morphology and localization. In particularly, US allows the distinction of different breast tissues and an increased spatial orientation.

Compared to real-time 2-D ultrasound, automated full-field three-dimensional breast ultrasound is an emerging modality for the detection and analysis of breast lesions. Acquisition of 3-D volumes facilitates follow-up diagnostics and separate reading, reproducibility of findings, intuitive coronal viewing and reading, as well as specific post-processing of image data. Hand-held 3-D US transducers generating cone-shaped image volumes are more common than automated full-field breast ultrasound scanners. Although the latter have been introduced nearly two decades ago, limited image quality and intricate handling prevented a widespread usage in routine diagnostics [1]. Recent 3DBUS systems employ upright or supine patient positioning and sequential full-volume imaging mechanisms, applying only slight compression to the breast. It was found that lesion diagnostics and findings in 2-D and 3-D breast ultrasound are almost equivalent, while individual criteria and specific phenomena differ between modalities [2,3].

D. Metaxas et al. (Eds.): MICCAI 2008, Part II, LNCS 5242, pp. 998–1005, 2008.

Dedicated software viewing systems for static and dynamic 3DBUS data have been proposed, easing the transition from 2-D US [4]. To support the radiologist's decision, computer-aided detection systems are currently being developed [5]. Furthermore, three-dimensional ultrasound is commonly used for interventional applications and particularly allows accurate biopsy needle guidance and placement [6]. Moreover, a system combining stereotactic MG and 3-D US for needle guidance was proposed by Fenster *et al.* [7].

Registration of breast images is an active field of research [8]. For 3-D ultrasound of the breast, a variety of methods have been proposed for compounding and multi-modality co-registration. Unlike 2-D US data, image volumes acquired by 3DBUS systems do not require reconstruction, although registered image volumes can be combined using dedicated image registration techniques [9,10,11]. Resulting compound images feature lower speckle noise and increased signal-to-noise ratio [12]. Compounding also generally facilitates multi-modality registration, for instance US-CT registration [13]. Xiao *et al.* [14] proposed a block-matching method for the non-linear registration of free-hand ultrasound, employing Bayesian regularization and B-spline interpolation to align individual 3-D scans. Block-matching for free-hand US was also presented by Boukerroui *et al.* [15] and Lin *et al.* [16]. Other methods for general elastic 3-D ultrasound registration have been proposed, such as a feature-based algorithm for liver US [17], dynamic registration to fuse cardiac MR and US [18], or a variational approach to US registration [19]. Notably, the majority of methods is targeted towards hand-held 2-D or 3-D US.

Due to an elongated acquisition time compared to conventional US, 3DBUS is prone to artifacts induced by the transducer sweep. This includes patient motion and breathing, tissue deformation enforced by transducer pressure variance, or readjustment of the transducer frame by the technician. Overall, linear slice motion and non-linear tissue distortions accumulate and produce distracting image artifacts, distinguishable from shadowing in the coronal view. Compensation of such distortions is crucial, particularly in the context of automatic image segmentation. Although breast motion is already restricted by a stabilizing membrane, deformations cannot be completely prevented. This issue is related to the compensation of free-hand 3-D US probe pressure proposed by Treece *et al.* [20,21]. However, the method was not applied to full-field 3DBUS volumes, assumes a convex pressure model and employs a different non-rigid registration sequence.

We demonstrate how a fast non-linear registration method effectively reduces motion artifacts in high-resolution full-field 3DBUS data. While not compensating missing image slices, the resulting corrected images display significantly more consistency. The employed method combines linear and elastic transformations into a single computational scheme in order to increase performance [22]. Unlike the method of Treece *et al.* [20], only one resampling step per iteration is required. Motion correction is performed by sequential registration of each slice onto adjacent image slices, enabling efficient on-line registration. We evaluated the algorithm on synthetically but reasonably distorted images and show that this alignment retains the original image structures and topologies. In a

first assessment, the method was qualitatively evaluated on 6 clinical datasets acquired with a U-Systems *SomoVu* 3DBUS system [1].

2 Method

Since the 3-D US volume is reconstructed from image slices acquired in subsequent transducer scans, motion correction will be based on sequential 2-D inter-slice registration. Spatial alignment of these slices requires the computation of global rigid transformations as well as local non-linear deformations.

2.1 Combined Registration Method

To compensate for both in-plane global motion of the scan slice and non-linear tissue deformation simultaneously, the transformation is separated into corresponding additive terms [22]. For a reference image $\mathbf{R}$ and a template image $\mathbf{T}$, at each coordinate $\boldsymbol{x} \in \mathbb{R}^3$ a global linear transformation $\boldsymbol{g}(\boldsymbol{x}, \boldsymbol{p}) = \boldsymbol{A_p x} + \boldsymbol{t_p}$, $\boldsymbol{g} : \mathbb{R}^3 \longrightarrow \mathbb{R}^3$ and a local non-linear image deformation $\boldsymbol{u}(\boldsymbol{x}) = (u_x, u_y, u_z)^T$, $\boldsymbol{u} : \mathbb{R}^3 \longrightarrow \mathbb{R}^3$ are computed. The linear transformation is determined by the parameters $\boldsymbol{p} = (p_1, \ldots, p_{12})^T$, with the translation defined by $\boldsymbol{t_p} = (p_{10}, p_{11}, p_{12})^T$. The error value

$$e(\boldsymbol{p}) = \frac{1}{2n} \sum_{i=0}^{n-1} \left[\mathbf{R}(\boldsymbol{x}_i) - \mathbf{T}(\boldsymbol{c}(\boldsymbol{x}_i, \boldsymbol{p}))\right]^2 \tag{1}$$

thus depends on the spatial image coordinates $\boldsymbol{x}$, the (combined) displacement coordinates $\boldsymbol{c}(\boldsymbol{x}, \boldsymbol{p}) = \boldsymbol{g}(\boldsymbol{x}, \boldsymbol{p}) + \boldsymbol{u}(\boldsymbol{x})$, and the two images, each with n voxels.

Equation (1) is minimized using a gradient-descent method [23]. Linear and non-linear partial derivatives are computed in each iteration, and parameter updates of linear parameters and local displacements are added using a linearly weighted convex combination [22]. Consistency of the non-linear deformation field is ensured by explicit *a posteriori* regularization, using either a discretized Gaussian [23,24] or linear elastic convolution kernel [25]. Finally, the computed deformation field is applied using trilinear interpolation.

2.2 Sequential Registration

The algorithm described in Sect. 2.1 is adapted to 2-D and employed for the 2-D registration of individual slices. Each slice is considered as a template image $\mathbf{T}_k$, where $k \in \{0 \ldots m\}$ denotes the current position in the 3-D image volume of $m + 1$ slices. For each template image, a reference slice $\mathbf{R}_k$ is chosen. In our evaluation we set

$$\mathbf{R}_k = \begin{cases} \alpha\mathbf{T}_0 + (1-\alpha)\mathbf{T}_2 & k = 1 \\ \alpha\bar{\mathbf{T}}_{k-1} + (1-\alpha)\mathbf{T}_{k+1} & 1 < k < m \\ \bar{\mathbf{T}}_{m-1} & k = m \end{cases} \tag{2}$$

as the reference for slice k, where $\bar{\mathbf{T}}_k$ denotes a registered image and $\mathbf{T}_0$ is not registered. Both the registered predeccessor $\bar{\mathbf{T}}_{k-1}$ and the successor $\mathbf{T}_{k+1}$ are

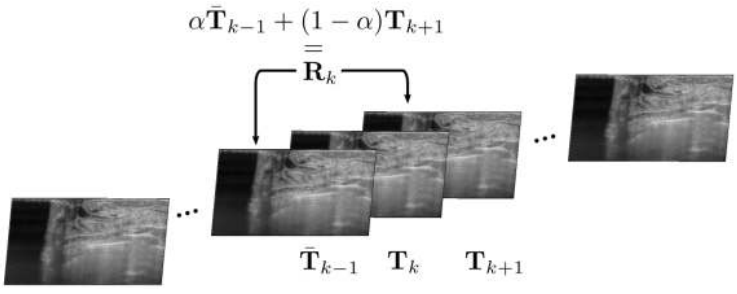

Fig. 1. Schematic illustration of the sequential registration procedure for a full 3-D US volume, showing the generated reference image $\mathbf{R}_k$ for the current template $\mathbf{T}_k$

considered in each registration, allowing an on-line application if desired (see Fig. 1). Factor α guides a convex combination of the two adjacent slices, and is set to

$$\alpha = \tau + |\hat{e} - e_k|^{\frac{1}{3}}(1-\tau), \qquad \alpha \in [\tau, 1], \tag{3}$$

where the error $e_k \in [0,1]$ is estimated using a normalized cross-correlation error of $\bar{\mathbf{T}}_{k-1}$ and $\mathbf{T}_k$. The summand $\tau \in [0,1]$ determines the range of α and is set to $\tau = 0.5$ for our evaluation. The power factor ensures a strong increase of alpha for outliers with high error deviations, and adjusts α adaptively w.r.t. the current error (see Fig. 2). The referenced error $\hat{e}$ is used for normalization w.r.t. the pronounced US noise. Since slices acquired first are typically not perturbed by motion, we set $\hat{e} = e_1$ to approximately estimate image noise. Furthermore, this optionally allows efficient on-line processing during acquisition.

The idea is to generate a stronger influence of the predecessor $\bar{\mathbf{T}}_{k-1}$ in α when $\bar{\mathbf{T}}_{k-1}$ is very dissimilar to the current image $\mathbf{T}_k$, and to relax this back to τ and an appropriately balanced weighting when the error decreases. If only $\bar{\mathbf{T}}_{k-1}$ would be referenced, all subsequent slices would be effectively registered to $\mathbf{T}_0$. Consequently, tissue layers would be over-registered and aligned linearly, rendering the US scan invalid (see Fig. 3). Crucial US features such as lesion shadows would be distorted. Furthermore, incremental registration errors would accumulate over time [20]. Combining information from both registered and

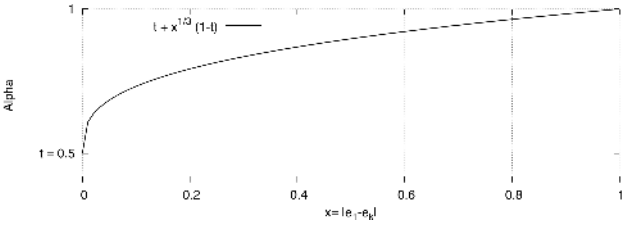

Fig. 2. Plot of the convex combination function α for $\tau = 0.5$

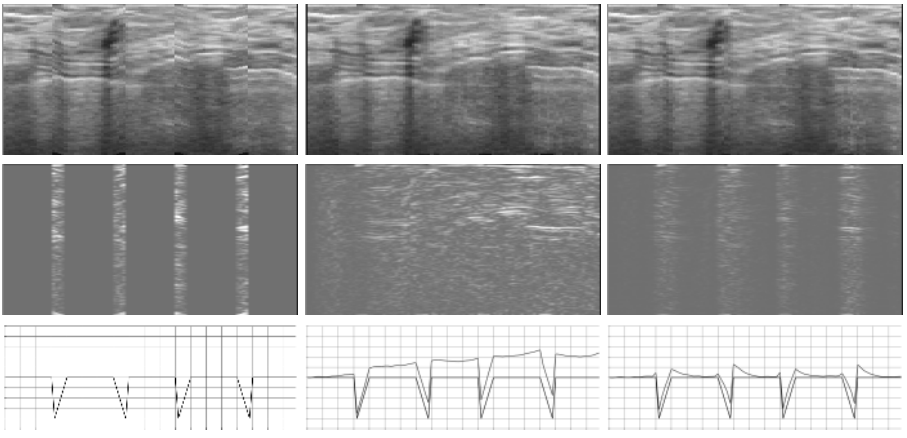

Fig. 3. Registration of artificially deformed data with sequential methods. Top row, left to right: Perturbed image, registered to predecessor only, registered using the adaptive weighting. Middle row: Corresponding absolute differences to the undeformed image. Bottom row: Optimal translation values (max. 4 voxels), and overlayed computed translation curves.

unregistered slices retains sufficient original image structures while reducing inter-scan inconsistencies.

3 Results

Quantitative and qualitative evaluation of the method was performed both on simulated images and actually distorted clinical images.

3.1 Artifical Deformations

To validate the method's accuracy, a known *a priori* deformation was applied to an exemplary dataset. A ramp translation offset (max. 4 voxels) was added to adjacent slices to model global slice motion. The perturbed and cropped image was registered with both methods: Using only the predecessor, and using the adaptive weighting described in Sect. 2.2. Results can be seen in Fig. 3.

Consideration of only the predecessor obviously results in significant tissue distortion caused by incremental registration errors, note the increasing curve difference. On average, the error was 1.48 ± 0.57 voxels with a maximum distance of 2.66 voxels. Inspection of the corresponding difference image confirms that errors accumulate over time, visible as increasing intensities towards the right.

The proposed adaptive weighting method performs significantly better, with an average distance of 0.38 ± 0.19 and a maximum distance of 1.51 voxels. The error between the two curves is considerably reduced and reaches its maximum directly adjacent to perturbations. The difference image is more consistent and reduces perturbations appropriately. Hence, for linear distortions accuracy of the proposed method even approaches imaging precision.

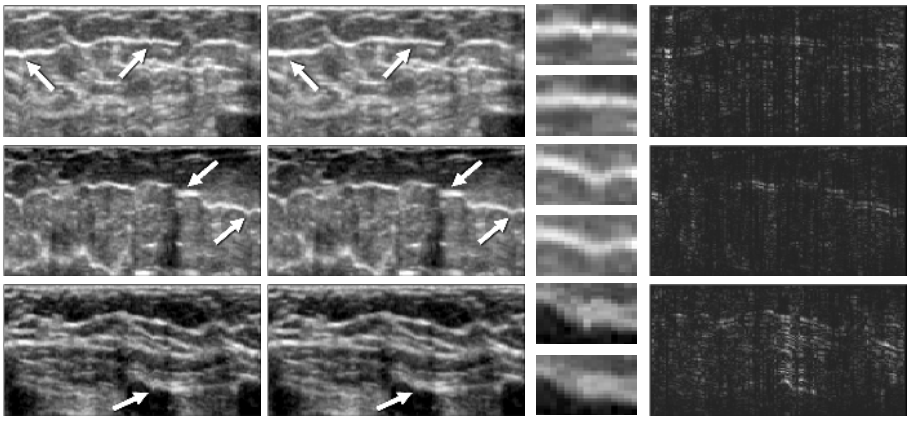

Fig. 4. Detailed sagittal view of three exemplary 3-D breast US datasets. From left to right: Original and registered images, details, and absolute difference of both images, highlighting changes after registration. Images courtesy of K. Schilling, BRCH, FL.

Contrary to quantitative assessment of computed linear deformations, rating of non-linear corrections is more complex. For elastic deformations, no gold standard is available yet, although finite-element model-based simulations provide valuable insight [26]. For a first assessment, an artificial non-linear deformation was added to the slice translation and distances between artifical and computed deformation fields were calculated. As for the linear part, the adaptive method again outperformed the simpler approach, with average distances of 0.27 ± 0.42 compared to 0.37 ± 0.41 voxels, and extreme distances of 1.89 and 2.08 voxels.

3.2 Clinical Images

For a preliminary assessment of the proposed method, totally 6 US datasets ($512 \times 185 \times 256$ voxels, $14 \times 5 \times 17\,\mathrm{cm}$) were registered, limited by the number of available datasets. On average, registration took 1.55 s per slice.

Resulting images were qualitatively reviewed by a trained radiologist, in direct comparison to the original images. Figure 4 shows three exemplary cases. Subjective ratings valued $r \in [1 \ldots 5]$ were assigned to each dataset and four different criteria (e.g., image quality), with $r = 5$ indicating perfect agreement. The proposed registration was robust and caused no distortions, thus consistency with the original data was rated 5 for all cases. Original image quality varied between 2.5 and 4, with an average of 3.2. General registration quality was rated as 4.3 on average, while artifact reduction was stated as 3.6. Although being purely subjective, this preliminary assessment confirms robustness and plausibility of the algorithmic strategy. Quantitative evaluation employing a sufficient number of datasets and accurate measurements, however, will provide detailed insight.

4 Discussion

We proposed an integrated linear and non-linear registration method for the reduction of motion artifacts in 3-D full-field breast US. The method uses an adaptively weighted combination of slices guided by noise estimation, and is suitable for on-line processing. Evaluation of the method on images with synthetic deformations produced small (< 0.5 voxels) mean errors. Strong agreement of expected and computed transformations was evidenced, in particular for linear motion. Preliminary qualitative assessment of the method resulted in no perceivable image degenerations and improved image quality.

For further work, a comprehensive quantitative analysis of the presented method is fundamental to confirm accuracy and robustness. Consequently, future work will integrate a larger set of data, along with techniques for quantitative assessment of registration errors using dedicated breast phantoms and deformations, and will identify consequences for lesion detection. Moreover, we will integrate dedicated US image similarity measures and investigate additional constraints, e.g., volume-preservation and temporal regularization. Further issues include an advanced pre-processing, analysis of registration w.r.t. US-specific noise and speckle, as well as additional improvement of algorithmic performance.

Acknowledgements. The authors would like to thank Dr. Benjamin Geisler, MeVis Research, for the qualitative image evaluation, and Dr. Kathy J. Schilling, Boca Raton Community Hospital, FL, for the kind contribution of US data.

References

1. Chou, Y., Tiu, C., Chen, J., Chang, R.: Automated full-field breast ultrasonography: The past and present. J. Med. Ultrasound 15(1), 31–44 (2007)
2. Cho, K., Seo, B., Lee, J., Pisano, E., Je, B., Lee, J., Choi, E., Chung, K., Whan Oh, Y.: A comparative study of 2D and 3D ultrasonography for evaluation of solid breast masses. Eur. J. Radiol. 54(3), 365–370 (2005)
3. Watermann, D., Foeldi, M., Hanjalic-Beck, A., Hasenburg, A., Lughausen, A., Prompeler, H., Gitsch, G., Stickeler, E.: Three-dimensional ultrasound for the assessment of breast lesions. Ultrasound Obstet Gynecol. 25, 592–598 (2005)
4. Weismann, C., Datz, L.: Diagnostic algorithm: How to make use of new 2D, 3D and 4D ultrasound technologies in breast imaging. Eur. J. Radiol. 64(2), 250–257 (2007)
5. Sahiner, B., Chan, H., Roubidoux, M., Hadjiiski, L., Helvie, M., Paramagul, C., Bailey, J., Nees, A., Blane, C.: Malignant and Benign Breast Masses on 3D US Volumetric Images: Effect of Computer-aided Diagnosis on Radiologist Accuracy. Radiology 242(3), 716–724 (2007)
6. Weismann, C., Forstner, R., Prokop, E., Rettenbacher, T.: Three-dimensional targeting: a new three-dimensional ultrasound technique to evaluate needle position during breast biopsy. Ultrasound Obstet Gynecol. 16(4), 359–364 (2000)
7. Fenster, A., Surry, K., Mills, G., Downey, D.: 3D ultrasound guided breast biopsy system. Ultrasonics 42(1-9), 769–774 (2004)
8. Guo, Y., Sivaramakrishna, R., Lu, C., Suri, J., Laxminarayan, S.: Breast image registration techniques: a survey. Med. Biol. Eng. Comput. 44(1), 15–26 (2006)

9. Rohling, R., Gee, A., Berman, L.: Three-dimensional spatial compounding of ultrasound images. Medical Image Analysis 1(3), 177–193 (1997)
10. Bashford, G., Morse, J.: Circular ultrasound compounding by designed matrix weighting. IEEE Trans. Med. Imag. 25(6), 732–741 (2006)
11. Wachinger, C., Wein, W., Navab, N.: Three-Dimensional Ultrasound Mosaicing. In: Ayache, N., Ourselin, S., Maeder, A. (eds.) MICCAI 2007, Part II. LNCS, vol. 4792, pp. 327–335. Springer, Heidelberg (2007)
12. Krucker, J., Meyer, C., LeCarpentier, G., Fowlkes, J., Carson, P.: 3D spatial compounding of ultrasound images using image-based nonrigid registration. Ultrasound Med. Biol. 26(9), 1475–1488 (2000)
13. Wein, W., Khamene, A., Clevert, D., Kutter, O., Navab, N.: Simulation and fully automatic multimodal registration of medical ultrasound. In: Ayache, N., Ourselin, S., Maeder, A. (eds.) MICCAI 2007, Part I. LNCS, vol. 4791, pp. 136–143. Springer, Heidelberg (2007)
14. Xiao, G., Brady, J., Noble, J., Burcher, M., English, R.: Nonrigid registration of 3-D free-hand ultrasound images of the breast. IEEE Trans. Med. Imag. 21(4), 405–412 (2002)
15. Boukerroui, D., Noble, J., Brady, M.: Velocity estimation in ultrasound images: A block matching approach. In: Proc. IPMI, pp. 586–598. Springer, Heidelberg
16. Lin, C., Weng, C., Sun, Y.: Ultrasound Image Compounding Based on Motion Compensation. In: Proc. IEE-EMBS, pp. 6445–6448 (2005)
17. Foroughi, P., Abolmaesumi, P., Hashtrudi-Zaad, K.: Intra-subject elastic registration of 3D ultrasound images. Medical Image Analysis 10(5), 713–725 (2006)
18. Zhang, W., Noble, J., Brady, J.: Spatio-temporal registration of real time 3D ultrasound to cardiovascular MR sequences. In: Ayache, N., Ourselin, S., Maeder, A. (eds.) MICCAI 2007, Part I. LNCS, vol. 4791, pp. 343–350. Springer, Heidelberg (2007)
19. Zikic, D., Wein, W., Khamene, A., Clevert, D., Navab, N.: Fast deformable registration of 3D-ultrasound data using a variational approach. In: Larsen, R., Nielsen, M., Sporring, J. (eds.) MICCAI 2006. LNCS, vol. 4190, pp. 915–923. Springer, Heidelberg (2006)
20. Treece, G., Prager, R., Gee, A., Berman, L.: Correction of probe pressure artifacts in freehand 3D ultrasound. Medical Image Analysis 6(3), 199–214 (2002)
21. Gee, A., Prager, R., Treece, G., Cash, C., Berman, L.: Processing and visualizing three-dimensional ultrasound data. Br. J. Radiol. 77(2), S186–S193 (2004)
22. Boehler, T., Wirtz, S., Peitgen, H.: A combined algorithm for breast MRI motion correction. In: SPIE Medical Imaging, vol. 6514, 65141R. SPIE Press (2007)
23. Pennec, X., Cachier, P., Ayache, N.: Understanding the Demon's Algorithm: 3D Non-rigid Registration by Gradient Descent. In: Taylor, C., Colchester, A. (eds.) MICCAI 1999. LNCS, vol. 1679, pp. 597–605. Springer, Heidelberg (1999)
24. Rogelj, P., Kovacic, S., Gee, J.: Validation of a nonrigid registration algorithm for multimodal data. In: SPIE Medical Imaging, vol. 4684, pp. 299–307. SPIE Press (2002)
25. Gramkow, C., Bro-Nielsen, M.: Comparison of Three Filters in the Solution of the Navier-Stokes Equation in Registration. In: Proc. SCIA, pp. 795–802 (1997)
26. Schnabel, J., Tanner, C., Castellano-Smith, A., Degenhard, A., Leach, M., Hose, D., Hill, D., Hawkes, D.: Validation of nonrigid image registration using finite-element methods: application to breast MR images. IEEE Trans. Med. Imag. 22(2), 238–247 (2003)